MICROPOROSITY IN RESERVOIR ROCKS: ITS MEASUREMENT AND INFLUENCE ON ELECTRICAL RESISTIVITY

PD: 11/1985
P: 42-52 (11)

B. F. SWANSON

We define micropores in reservoir rocks as pores whose dimensions are significantly smaller than those contributing to the rock's permeability. They are contained, for example, between the crystals of clay in shaly sands, and within porous chert grains. The relative volume of these micropores is a major factor controlling water saturation in oil and gas reservoirs.

MEASUREMENT TOOLS

Mercury Porosimetry

We employ the Micromeritics autopore 9200 porosimeter for capillary pressure measurements up to about 55,000 psi. This pressure is sufficient to detect cylindrical capillaries of about 0.004 μm diameter. The device was intended for use in the powder and catalyst industries. Thus it is not an optimum tool for reservoir studies, but it has been adapted.

The instrument performs, semi-automatically, injection of mercury at programmed pressure steps from less than one psi to 55,000 psi. Four samples are measured at once for pressures up to 24 psi. Then two at a time are monitored from 24 psi to 55,000 psi. Data are stored for transmission at the completion of each test.

The rock samples are placed into individually calibrated glass penetrometers. The penetrometers consist of a sample chamber and precision-bore glass capillary whose volume is selected to be just larger than the expected pore volume of the rock. The outside of the glass capillary is plated with metal which acts as one plate of a capacitor. The mercury within the capillary acts as the other capacitance plate. Volume injection of mercury is monitored by capacitance bridges.

For pressures up to 24 psi, air pressure is used. Hydraulic oil is used for the higher pressures. No volume corrections for pressure effects on the equipment are used. They are assumed negligible for pressures below 24 psi. For high pressures, the penetrometer experiences equal external and internal pressures. Mercury compression is assumed to be offset by penetrometer compression. In principle, the latter is only true for a particular volume of sample.

Mercury volumes are expressed in cubic centimeters mercury per gram dry weight of rock. A tabular output is produced. Pore size is computed using the La Place equation for cylindrical pores. An accumulative volume injection curve is plotted. See Figure 1. The differential (or incremental) volume curve of Figure 2 is particularly useful for interpreting interconnecting pore dimensions.

The examples shown in Figures 1 and 2 were measured on a sandstone containing intergranular porosity and microporosity within both kaolinite clay and chert. Using Figure 2, the intergranular pore network which contributes the rock's permeability shows a peak in pore diameter at 42 μm. Kaolinite pore interconnections peak at around 3 μm, whereas the chert pores are much smaller, peaking at about 0.1 μm.

Note the dip in Figure 2 at a pore size of 5.96 μm. This is associated with the pressure transition from low range to high range. The penetrometer is physically moved from a low pressure cell to a high pressure cell. There are orientation and hysteresis effects which the computer software often fails to correct. This can be a serious problem should the transition pressure be on the plateau of the capillary pressure curve. This dip is commonly observed in measurements on permeable rocks. Micrometrics offer suggestions for minimizing these errors.

Scanning Electron Microscopy (SEM)

SEM photographs such as the kaolinite and chert in the previous example, can be used to interpret pore size range as well. See Figure 3. Note the pores in the kaolinite area are far more plate-like than cylindrical. For the case of pores with a large dimension many times larger than the smallest dimension, the calculated narrow dimension should be about half that computed for a cylindrical pore. From Figure 2, the transition to mercury intrusion into the kaolinite begins at about 4.8 μm (one half of 9.7 μm). Intrusion continues over a broad size range to 1.5 μm. (one half of 3 μm.) at the peak. This range of crystal spacings is comparable to the visual range observed in Figure 3. The same comparison may be made for the porous chert. Keep in mind that the capillary pressure-derived pore dimensions apply to the interconnecting pores.

Water/Oil Capillary Pressure Tests

Water/oil capillary pressure measurements are made using the capillary plate method. The equipment is essentially the same as described previously (Waxman & Thomas, 1974). One variant, however, is that water-wet porous vycor plates are sometimes used. Because of ex-

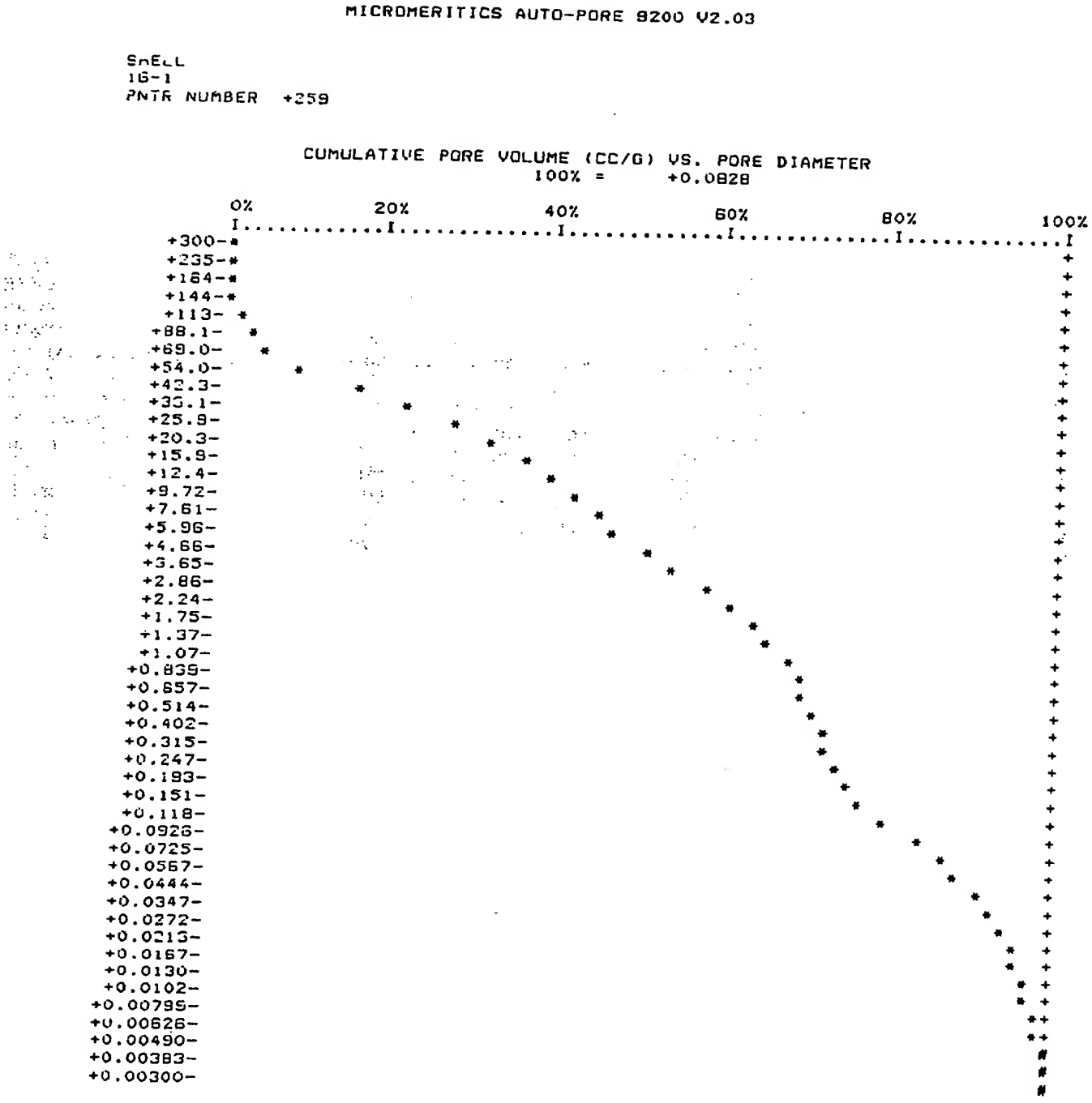

Figure 1: Micromeritics autopore output: Accumulative volume of mercury injection versus pore size. The accumulative pore volume is expressed as a percentage of the total mercury injected at maximum capillary pressure.

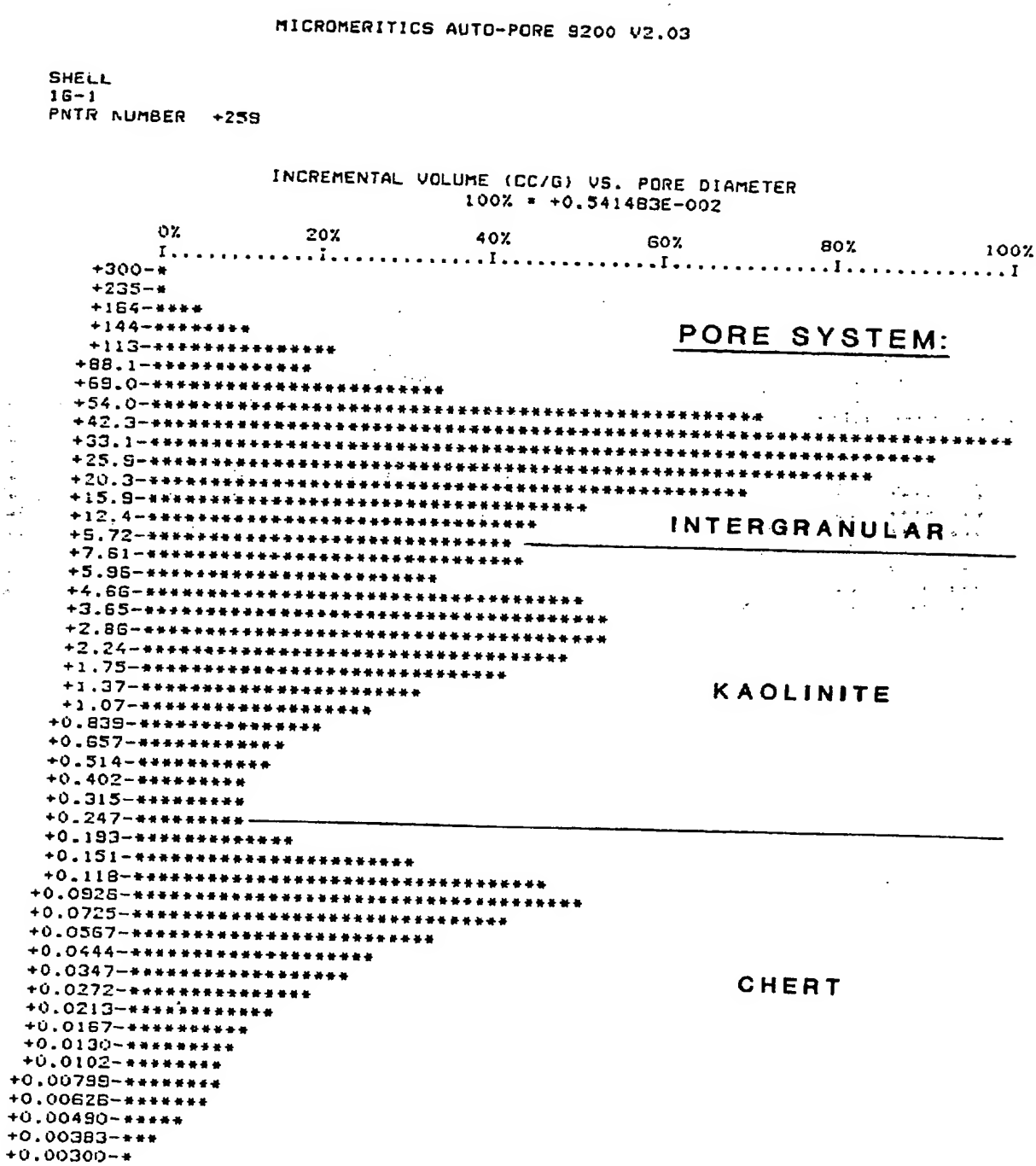

Figure 2: Micromeritics autopore output: Incremental volume of mercury injected versus pore size. The accumulative pore volume is expressed as a percentage of the total mercury injected at maximum capillary pressure.

Kaolinite

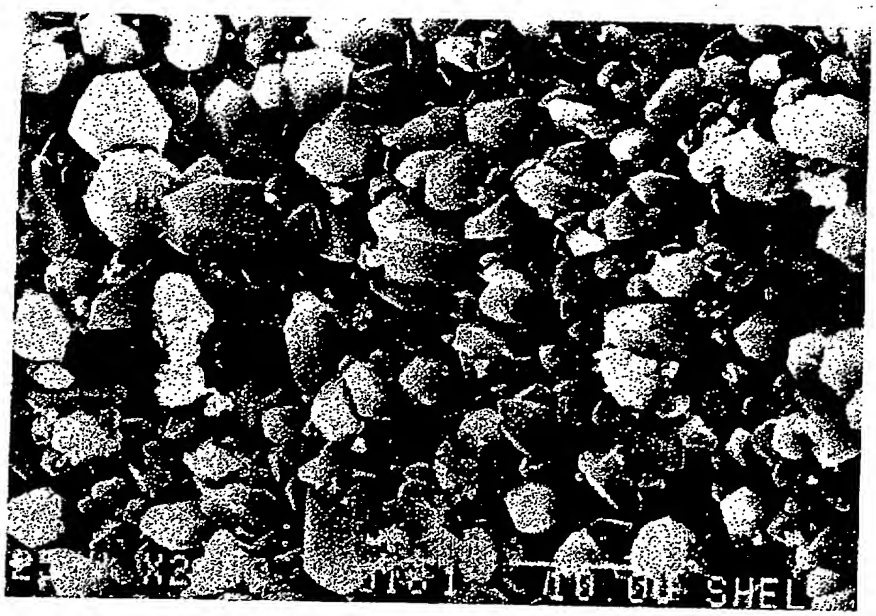

Chert

Figure 3: Scanning electron microphotograph of micropores in kaolinite and chert for the sample of Figures 1 and 2.

tremely small pore size, these plates allow desaturation of reservoir rocks at water/oil capillary pressures up to 500 psi using white oils. Tests are very slow using these plates. More commonly, ceramic plates with larger pore sizes are used.

Differences between capillary pressure curves derived from mercury and water/oil tests can often be attributed to a lack of equilibrium in the water/oil tests. This is particularly true when water saturation has been reduced substantially at higher capillary pressures. Difficulty in attaining equilibrium is attributed to the ever-diminishing relative permeability to water at decreasing water saturations.

By taking precise data frequently, we can estimate an equilibrium water saturation for a specific capillary pressure. We plot water saturation versus time in such a way that we can graphically determine the slope of the curve (ds/dt). A log-log plot of ds/dt versus t shows that for later times, a linear trend with slope well below minus one develops. See Figure 4. This indicates convergence. By integrating the equation of this linear region between the limits of the last time step to infinite time yields the desaturation needed to attain equilibrium. In this example, an additional desaturation of .008 pore volumes is estimated even after 46 hours.

For capillary pressures high enough to cause oil penetration into isolated clumps of microporosity, such as found in chert, very long times are required to develop the linearity in the ds/dt versus t curve. Large saturation extrapolations are usually computed as well. This is due to the relative water permeability in the surrounding matrix being very low, and a large volume of water to transport.

INFLUENCE OF EFFECTIVE STRESS

Capillary pressure relationships are useful to estimate hydrocarbon saturations in a reservoir provided sufficient information about the rock and contained fluids is available. We must be assured that the state of the rock during a capillary pressure test is representative.

For sandstones containing abundant chlorite, a mercury capillary pressure curve such as in Figure 5 is found. The micropore system is arbitrarily defined as pores with entry pressures greater than found at the inflection point in the first steeply rising region of the capillary pressure curve. The macropores are those entered by mercury below this pressure. The latter contribute to hydrocarbon oil storage volume and permeability. Note that the inflection point occurs at about 300 psi mercury pressure in this example and is thus visible in the standard 1000 psi capillary pressure curves obtained from equipment such as is available from Ruska Engineering.

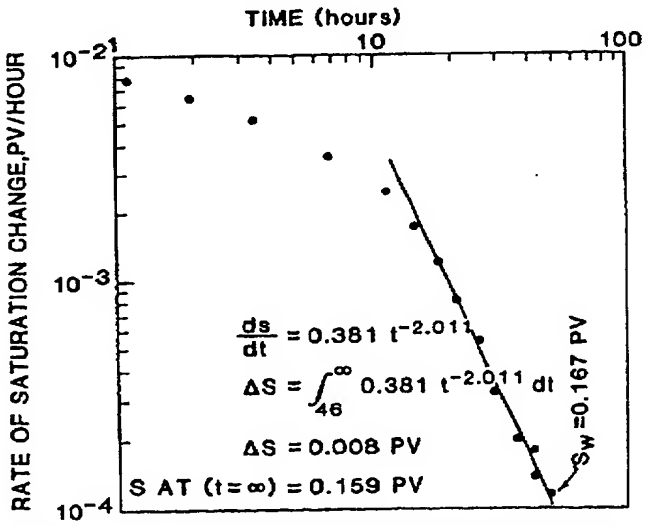

Figure 4: Equilibrium saturation by data extrapolation.

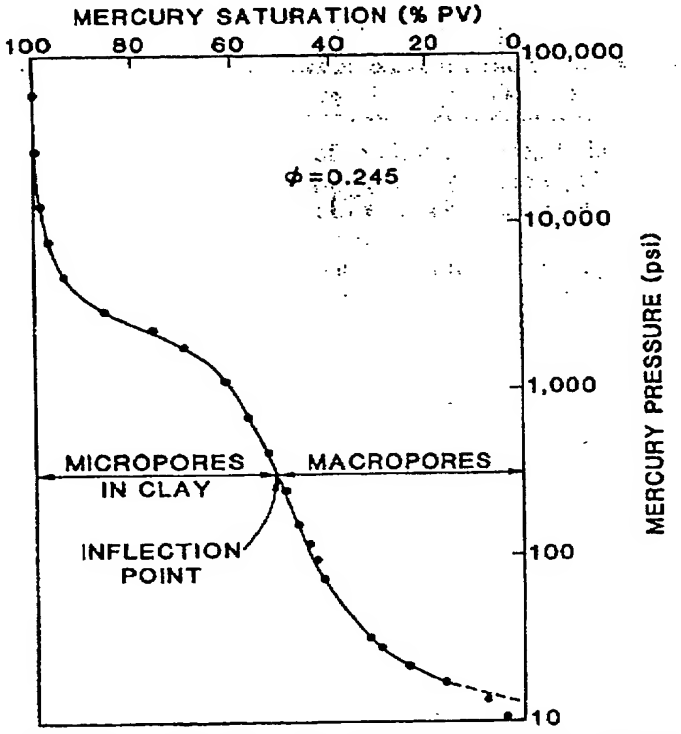

Figure 5: Definition of microporosity from capillary pressures.

The chlorite druse in the sandstone of Figure 5 is authigenic. Clay crystals have grown within an existing pore system, reducing its porosity. The clay should not be bearing the load of the overlying rock. Upon release of in-situ stress by coring, the volume of pore system within the clay should be essentially unaffected. Any increase in porosity due to stress relief occurs in the macropore system of the rock.

We shall assume that the porosity measured on a water/oil capillary pressure sample under confining pressure is representative of in-situ conditions. We can make a first order stress correction to mercury saturation data using the technique pictured in Figure 6.

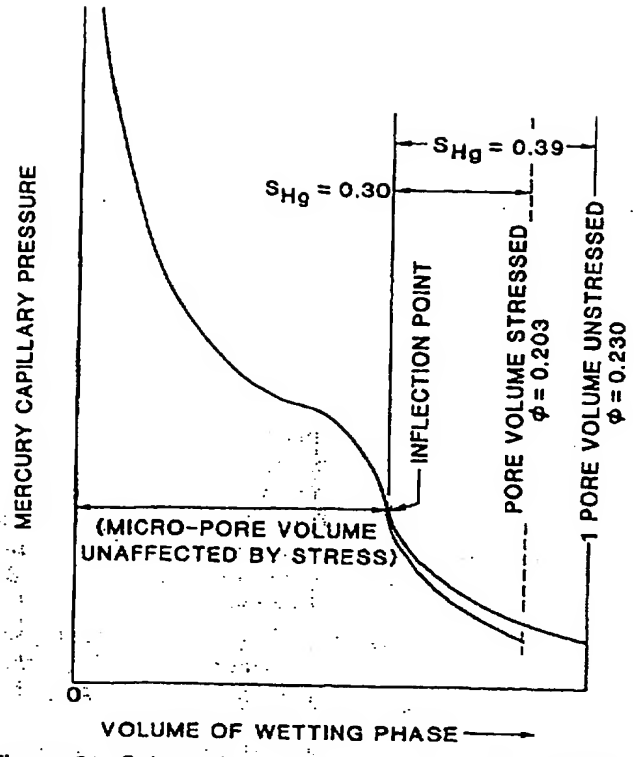

Figure 6: Schematic method of correcting capillary pressure data for stress effects.

The micropore volume per unit grain volume remains unaffected by stress as argued previously. the macropores are reduced in volume by the amount of porosity reduction due to lab stress, ϕ = .238 to ϕ = .203 in this example. The mercury saturation changes from 0.39 to 0.30 at the inflection point of the capillary pressure curve. The shape of the stress-corrected capillary pressure curve between entry pressure and inflection point is proportioned as defined by the unstressed curve. No pressure corrections are made in this simplistic approach.

Consider the capillary pressure curves, Figure 7, for a chloritic sandstone. One was determined using mercury on an unstressed sample, corrected for stress effect, the other using water and oil on a stressed sample. The two curves have been normalized by interfacial tensions, as described in the next section. Now the two techniques yield excellent agreement.

NORMALIZED CAPILLARY PRESSURES

We now compare the mercury capillary pressure curve corrected for stress restoration with water/oil data.

A plot of capillary pressure divided by interfacial tension (γ) should yield identical results for various pairs of wetting and nonwetting phases, all other effects being accounted for. However, the effective contact angle θ is a complicating factor. It is usually accounted for by multiplying interfacial tension by the cosine of the contact angle.

The pore surfaces within the macropores in this chloritic sand are extremely rough due to the pore-lining chlorite druse. The effect of this rough surface is to produce a severe hysteresis in the contact angle, depending on the direction of motion of the interface. Morrow (1975) has shown the magnitude of this effect in measurements on etched capillaries as well as textured bead packs. Figure 8 is a modified version of his results.

Mercury contact angles on smooth quartz surfaces are found to be 130° to 140°, measured through the mercury phase. The wetting phase (vacuum) angle thus is 40° to 50°. From Figure 8, we see that on a rough surface, the active cos θ for a 40° to 50° contact angle on smooth surfaces is 1.0, the value for a strongly wetting system. In the figure, drainage capillary pressures would be following the accumulating oil cycle. Thus for our mercury data, a value of cos θ = 1.0 applies. this should also be true for the water-oil case, as Soltrol, a nonpolar oil, was used in these tests.

The interfacial tension in mercury-vacuum systems has been measured to be 484 dynes per centimeter. The interfacial tension in our brine/soltrol system was measured by duNouy tensiometer to be 44.5 dynes per centimeter.

The stress corrected mercury capillary pressure data from Figure 7 and the water/oil P_c data on the same sample are plotted versus normalized capillary pressures, P_c/γ, in Figure 9. This striking agreement suggests there is merit to the techniques and assumptions that were used. This agreement has been observed for several samples of chloritic sandstone.

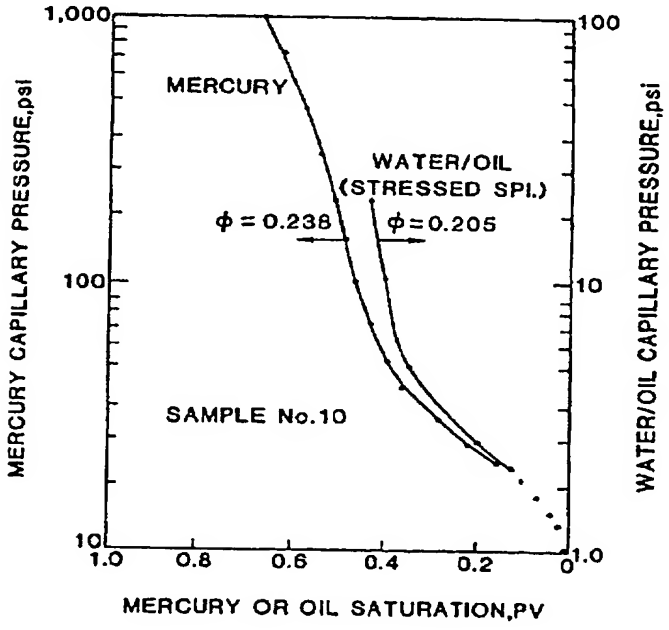

Figure 7: Comparison of mercury and water/oil capillary pressures.

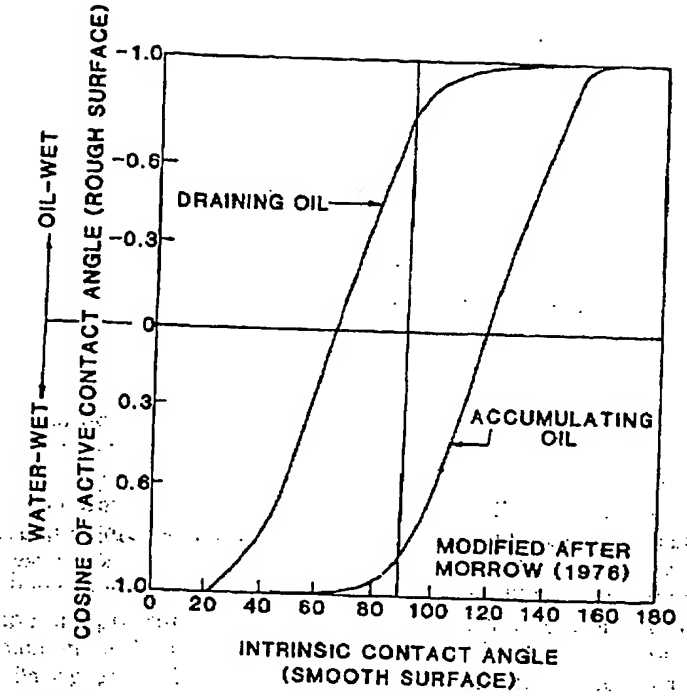

Figure 8: Influence of surface roughness on effective cosine of contact angle.

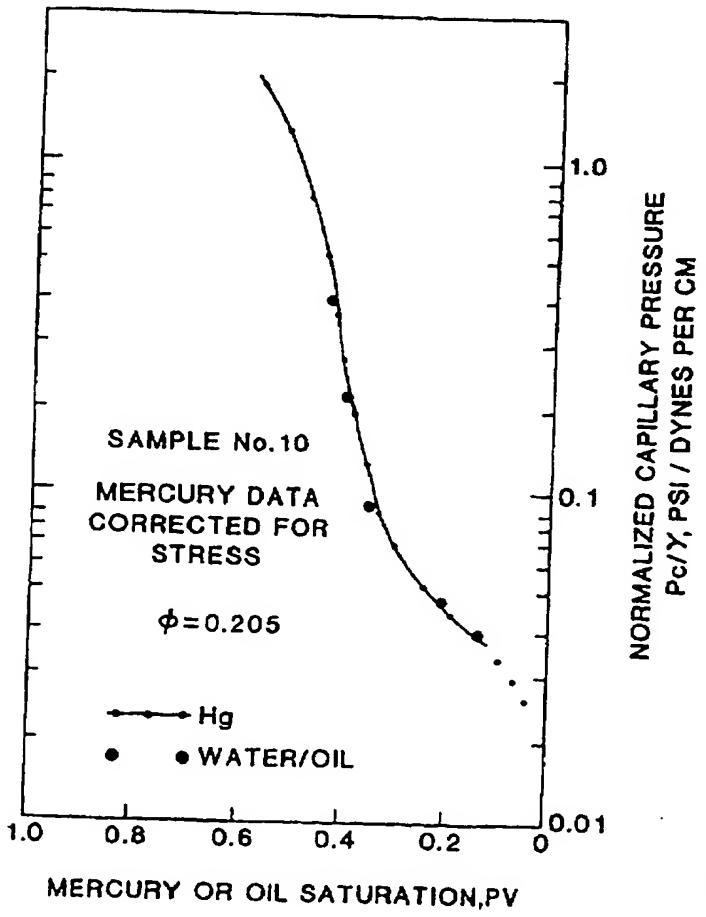

Figure 9: Comparison of normalized, stress-corrected mercury data with water/oil data.

INFLUENCE OF MICROPOROSITY ON ELECTRICAL RESISTIVITY

The relationship between resistivity index and brine saturation is measured with the same equipment as is used for water/oil capillary pressure tests. Both measurements may be determined simultaneously.

Figures 10-13 show resistivity index versus water saturation and mercury capillary pressure curves for four sandstones containing varying amounts and types of microporosity. Note that at the saturation where mercury penetration into microporosity occurs, the resistivity index relationships change slope. For the case where the microporosity occurs in isolated clumps, as in detrital chert grains, one can argue that all electrical current passing through a porous grain must have also passed through regions of surrounding matrix containing no microporosity. This suggests a series electrical circuit may be required to model this network.

Consider the model capillary pressure curve shown in Figure 14 as being represented by two capillary pressure curves, one for the macropores, the other for the micropores. The macropores contain 80% of the total pore space, the micropores 20%. Assigning a value of 1.7 for an Archie saturation exponent for both pore systems and assuming equal porosity in the two, we can calculate a resistivity index curve, assuming a series electrical circuit. This is done by summing the resistivity ratios of the two pore systems in proportion to their volumes and saturations for various positions on the capillary pressure curves. Figure 15 shows the resulting relation between I and S_w.

Even though this is a very simplistic model, the form of the curve is reflected in the data of Figures 12 and 13, in both of which we find porous detrital chert the dominant micropore system.

To conceptualize this electrical behavior, consider that, as oil saturation increases, first the resistivity is dominated by the larger pore network (the larger resistor in the series circuit). Water saturation is large because of the microporosity. A high apparent saturation exponent n results. Then as capillary pressure increases sufficiently to penetrate the micropores, water drains from the micropores with very little influence on resistivity. Apparent n decreases.

For the samples of Figures 12 and 13, I versus S_w relations were measured with more than one saturating brine salinity. An effect attributable to clay conductance is observed. Most of the previous I versus S_w data available to us for appraising Waxman-Smits (1968) behavior at reduced water saturation was obtained for capillary pressures below the micropore entry pressures. Using I versus S_w data for the higher water saturations, we have computed n* and the resulting Waxman-Smits I versus S_w relations for the cherty sample as shown in Figure 13. The cation exchange capacity (Q_v) for this sample is a quite low 0.042 meq/ml.

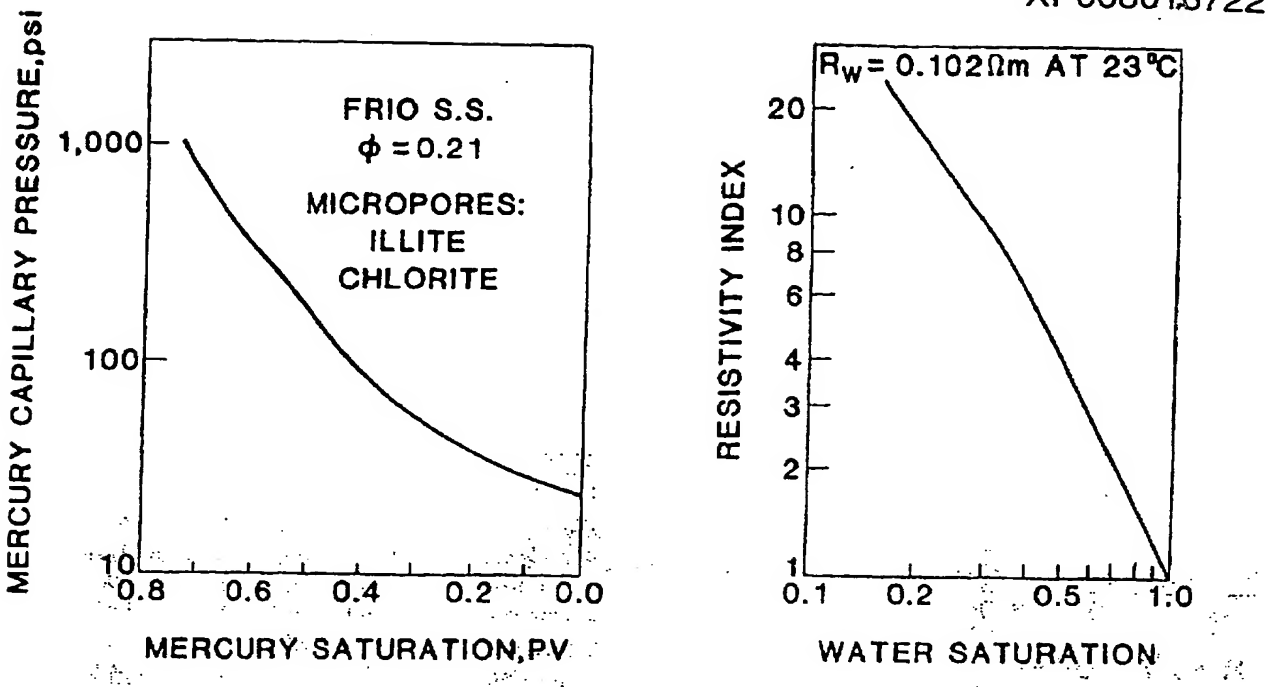

Figure 10: Capillary pressure and I versus S_w for a Frio sandstone.

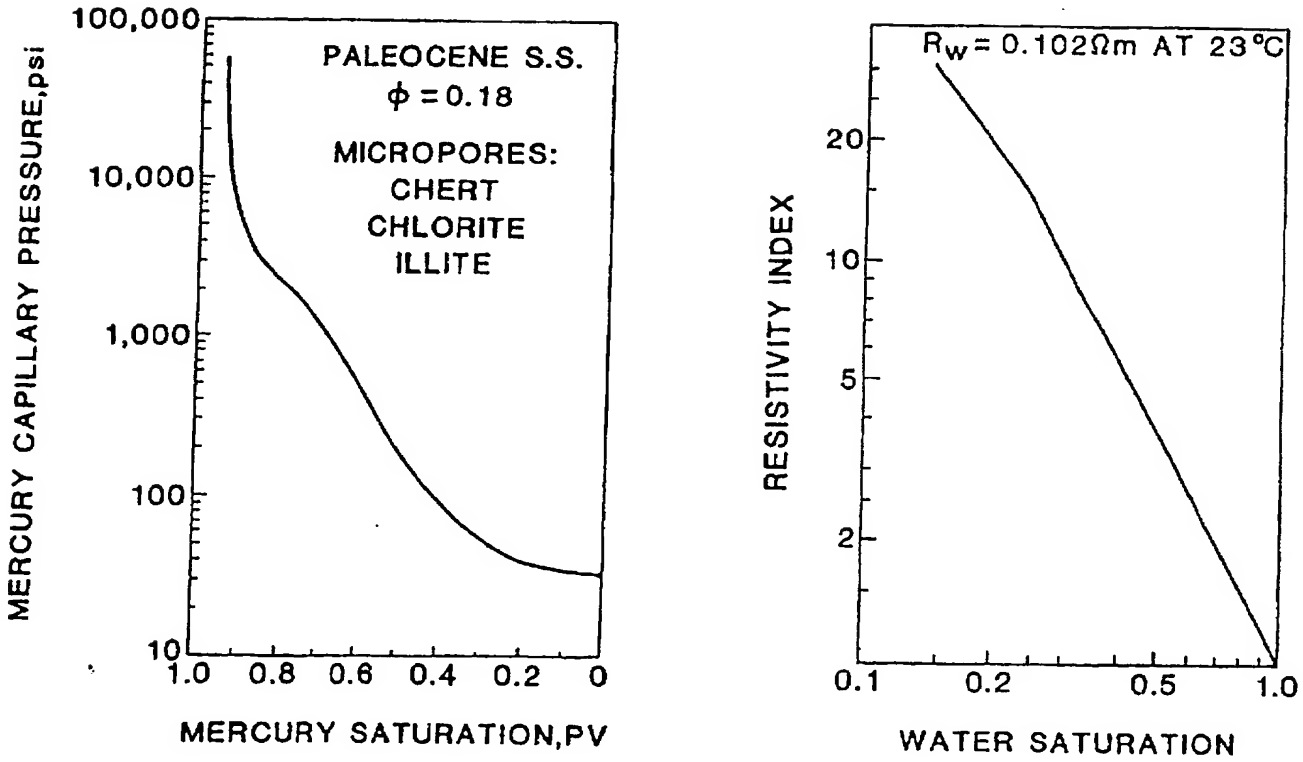

Figure 11: Capillary pressure and I versus S_w for a Paleocene sandstone.

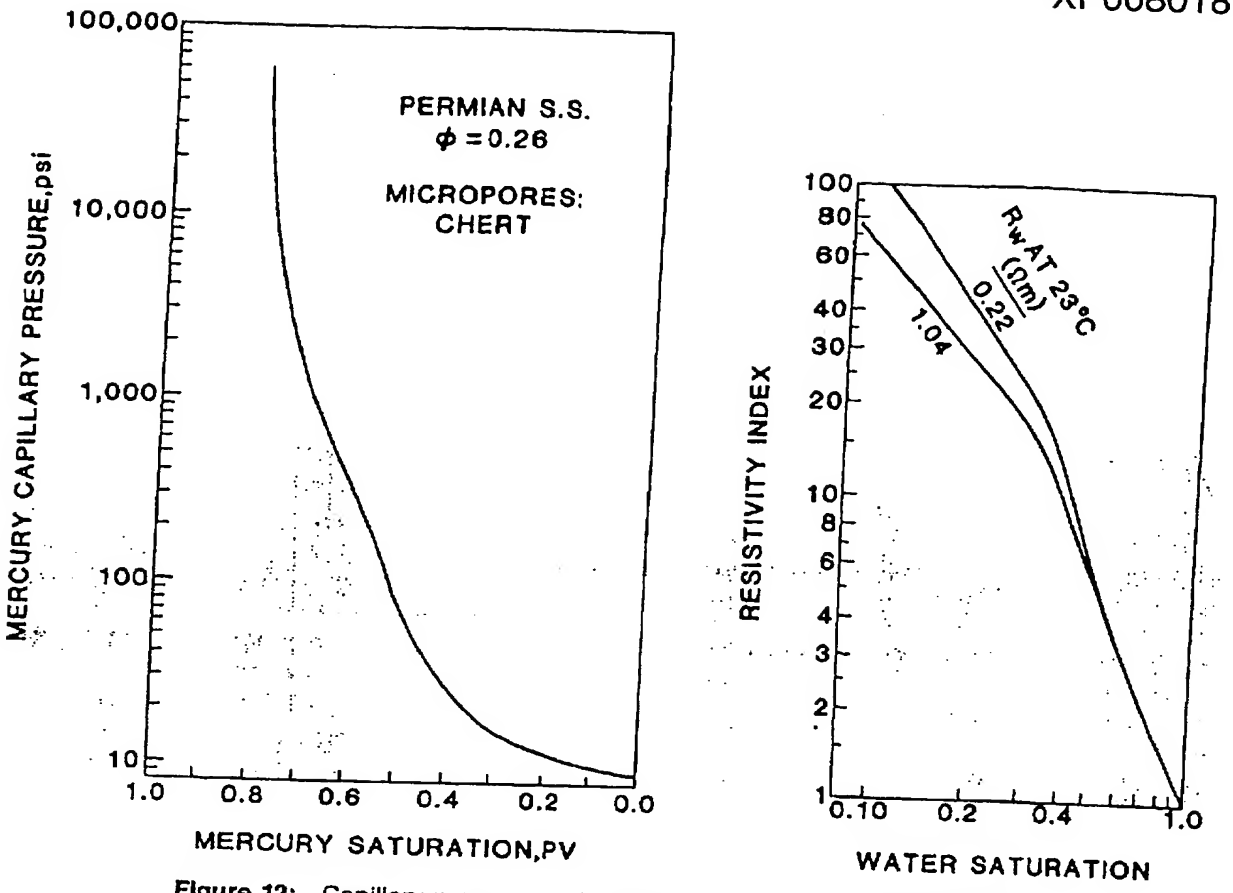

Figure 12: Capillary pressure and I versus S_w for a Permian sandstone.

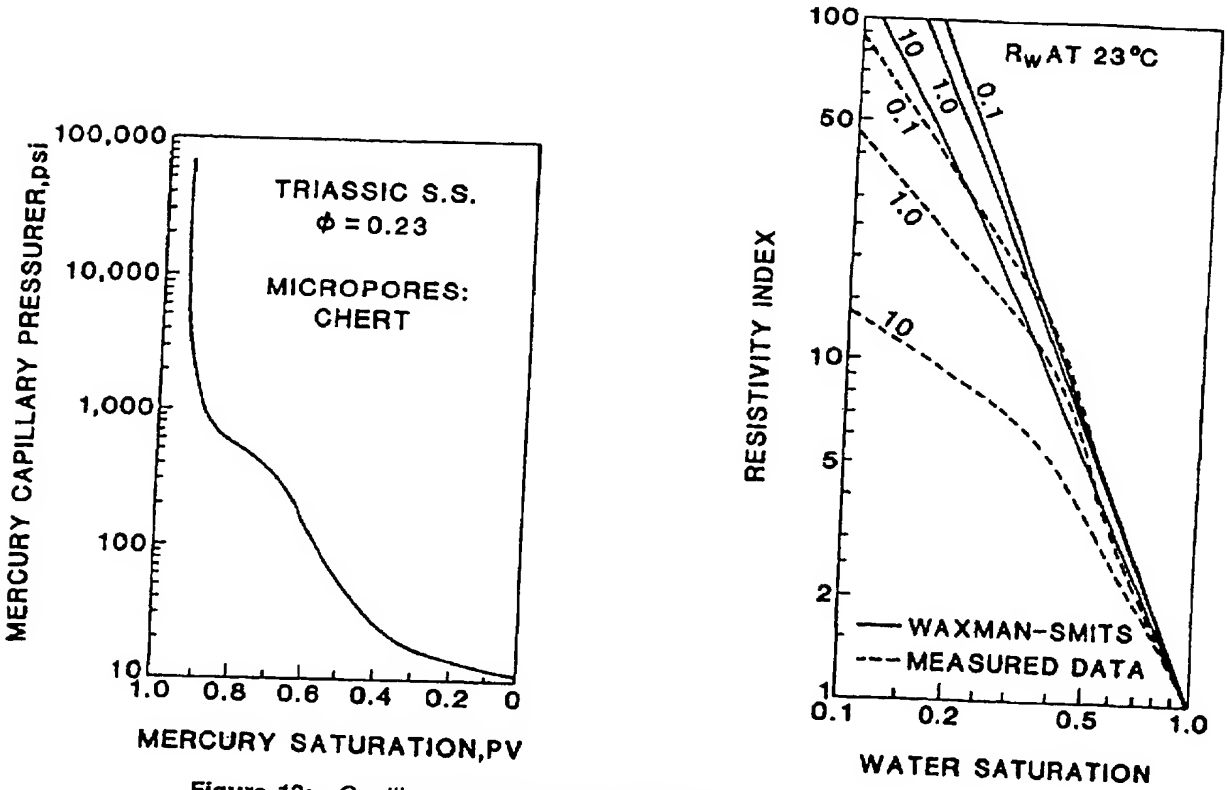

Figure 13: Capillary pressure and I versus S_w for a Triassic sandstone.

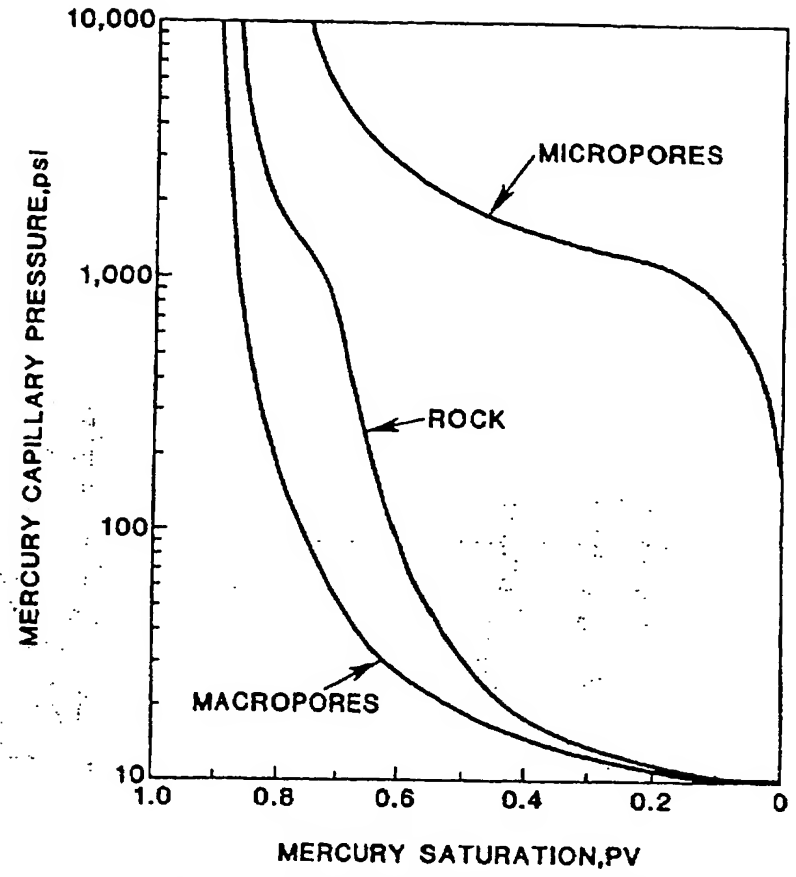

Figure 14: Separation of capillary pressure curve into macropores and micropores.

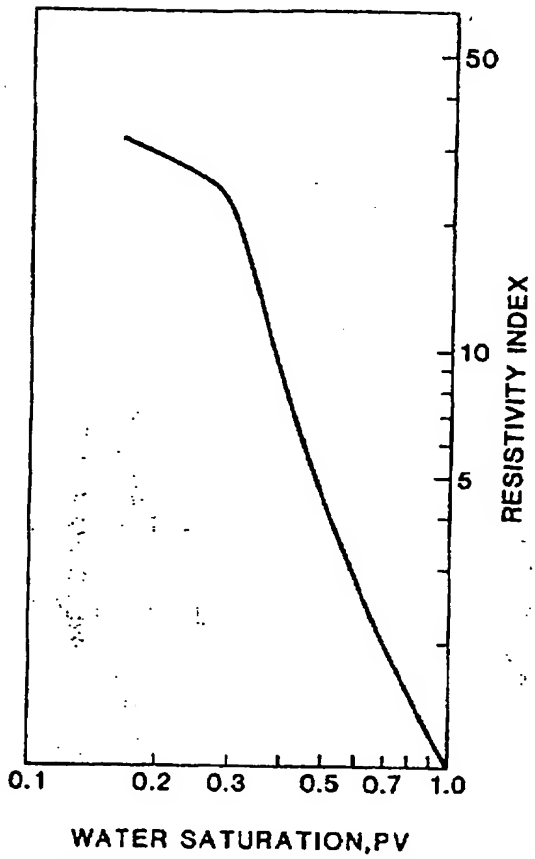

Figure 15: Modeled I versus S_w curve for series electrical circuit.

The Waxman-Smits curves deviate substantially from the measured data at lower water saturations, particularly at low salinities. This is apparently due to their model's neglect of capillary water in micropores and the degree to which that microporosity is isolated. Morphology appears to be much more important in electrical behavoir at reduced water saturation than the Q_v/S_w assumption of Waxman-Smits accounts for.

We believe a third type of electrical conductance is complexed with pore water in the primary pore network and with clay counter-ion conduction. This water is capillary water within porous grains and clay structures. Many of our rock types contain porous chert grains and cement. The pore systems associated with these minerals appear from SEM analyses to be relatively isolated from each other electrically. In this state, they must exist in a series electrical manner with other pore water, rather than parallel as with the Waxman-Smits model for counter-ion conduction. Thus when water is drained from these finer pores at higher capillary pressure, a much less significant increase in resistivity occurs (lower Archie n), and the I versus S_w curve bends sharply to another trend.

CONCLUSIONS

1. Microporosity can be found in siliciclastics within clays and chert.
2. High pressure mercury porosimetry is useful in determining the relative proportion of microporosity in reservoir rocks.
3. Lack of saturation equilibrium can cause a significant difference between water/oil and mercury capillary pressure curves. Equilibrium water/oil saturations may be estimated by extrapolation to infinite time of rate of change of saturation.
4. Capillary pressure data measured on rocks containing non-load-bearing microporosity show a significant dependence on sample confining pressure. A first order correction to capillary pressure data for these rocks may be made when the porosity of the stressed rock is known.
5. Water/oil capillary pressure data on chloritic sandstones measured with confining pressure agree with stress-corrected mercury data when normalized by interfacial tensions.
6. When oil begins to penetrate micropore systems in

measurements of resistivity index versus brine saturation, a significant change in slope of the I versus S_w data occurs.

7. I versus S_w data for rocks containing a significant volume of microporosity deviates substantially from Waxman-Smits behavior when the capillary pressure is high enough for oil content in the micropores.

REFERENCES

1. Waxman, M. H. and Thomas, E. C. (1974) Electrical Conductivities in Shaly Sands, Journal of Petroleum Technology, February.
2. Morrow, N. R. (1975) The Effects of Surface Roughness on Contact Angle With Special Reference to Petroleum Recovery, J. Canadian Petroleum Technology, v. 14, October – December, 42-53.
3. Waxman, M. H. and Smits, L. J. M. (1968) Electrical Conductivities in Oil Bearing Shaly Sands, SPE Journal, June.

ABOUT THE AUTHOR

Ben F. Swanson is a senior staff research physicist with Shell Development Company's Bellaire Research Center in Houston, Texas. He holds a BS degree in Physics from the University of Houston. For 33 years, Swanson has been involved in research of rock properties associated with well logging, fluid flow, rock mechanics and core analysis. His paper, "Microporosity In Reservoir Rocks: Its Measurement And Influence On Electrical Resistivity," won the Best Paper Award at the SPWLA Twenty-sixth Annual Symposium.